Journal of Materials Chemistry B

ROYAL SOCIETY OF CHEMISTRY

PAPER

View Article Online
View Journal | View Issue

Cite this: J. Mater. Chem. B, 2025, 13, 5957

Illuminating apoptosis: a visible light-activated chloride carrier for chloride transport and cell death†

Manzoor Ahmad, ‡[a] Naveen J. Roy,[a] Debashis Mondal,§[a] Thangavel Vijayakanth,[c] Mayurika Lahiri[b] and Pinaki Talukdar *[a]

Received 30th October 2024,
Accepted 1st April 2025

DOI: 10.1039/d4tb02436b

rsc.li/materials-b

Synthetic chloride carriers are known to induce chloride-mediated apoptosis inside cancer cells. One of the main disadvantages is the unfavorable cytotoxicity towards healthy cells due to the lack of selectivity. The use of stimuli, such as light, enzymes, ligands, *etc.*, has enabled the selective activation of these systems in cancer cells. Light, notably, is a significant stimulus that has been utilized due to its excellent spatiotemporal control, remote addressability, and low cytotoxicity. However, previously reported photoresponsive systems require UV radiation for their activation, which has low tissue penetration and can lead to phototoxic cell damage or death. Herein, we report 3-substituted indole-2-carboxamide ion carriers and their *o*-nitrobenzyl (ONB) linked procarriers. The incorporation of the electron-donating substituents to the ONB photocleavable group leads to a significant red shift in the absorption wavelength, and for the *N*,*N*-dimethyl-based procarrier, the absorbance peak extends up to 500 nm. Eventually, all the synthesized procarriers were photoactivated inside MCF-7 cancer cells under 400 nm electromagnetic radiation, and the *N*,*N*-dimethyl-based procarrier was also photoactivated at 450 nm. This photoactivation at a higher wavelength of electromagnetic radiation is highly desirable for its practical biological applications.

Introduction

Cancer is one of the leading causes of death worldwide. Traditional anticancer drugs used in chemotherapy have multiple adverse effects, including immunosuppression, neutropenic enterocolitis, anemia, infertility, *etc.*[1–3] Furthermore, these drugs usually target specific enzymes/proteins in the cancer cells or disturb the fundamental DNA replication processes to eliminate the malignant cells.[4,5] Therefore, the resistance developed by the cancer cells through the activation of anti-apoptotic pathways,[6] *e.g.*, mutation of the drug-targeting sites,[7,8] overexpression of genes and proteins, *etc.*,[9] is known to curb their therapeutic effectiveness. Dysregulation of ion homeostasis, particularly for calcium,[10] potassium,[11] and chloride,[12,13] is known to be closely related to the onset of apoptosis. Various natural and artificial chloride carriers are known to perturb chloride ion homeostasis and lead to apoptotic cell death of cancer cells. These include prodigiosin,[14] tambjamine,[15] calix[4]pyrroles,[16] urea/thioureas,[17,18] bis-sulfonamides,[19] and squaramides,[20] among others. Unlike binding to specific enzymes or proteins, these molecules function in the lipid membrane and hence, can overcome the resistance issues related to the mutation and overexpression of genes and proteins in cancer cells. However, the cytotoxicity towards normal cells is a limitation to their use in anticancer therapy. In this regard, many stimulus-responsive ion transport systems have been reported that can selectively activate inside the cancer cells without affecting the normal healthy cells. The stimuli include the use of pH variations,[21–25] enzymes,[26] ligands/metabolites,[27–30] and light[31] among others.[32–35] However, very few stimuli-responsive ion transport systems are known to be selectively activated inside cancer cells.[36–41] Light-responsive ion transport systems, in particular, are

[a] Department of Chemistry, Indian Institute of Science Education and Research Pune, Dr Homi Bhabha Road, Pashan, Pune 411008, Maharashtra, India. E-mail: ptalukdar@iiserpune.ac.in
[b] Department of Biology, Indian Institute of Science Education and Research Pune, Dr Homi Bhabha Road, Pashan, Pune 411008, Maharashtra, India
[c] The Shmunis School of Biomedicine and Cancer Research, George S. Wise Faculty of Life Sciences, Tel Aviv University, Tel Aviv 6997801, Israel

† Electronic supplementary information (ESI) available: Details of synthetic protocols and characterization of compounds, crystallographic parameters, experimental protocols, including vesicle preparation, ion transport assays and biological studies, additional data for ion transport studies, details of geometry optimized structures and additional biological data. CCDC 2127603(5′), 2127604(5′), 2155430(**5a**), 2127605(**5c**), 2127606(**5d**) and 2127607(**6e**). For ESI and crystallographic data in CIF or other electronic format see DOI: https://doi.org/10.1039/d4tb02436b

‡ Present address: Chemistry Research Laboratory, Mansfield Road, Oxford, OX1 3TA, UK.
§ Present Address: Department of Chemistry, University of Reading, Whiteknights, Reading, RG6 6DX, UK.

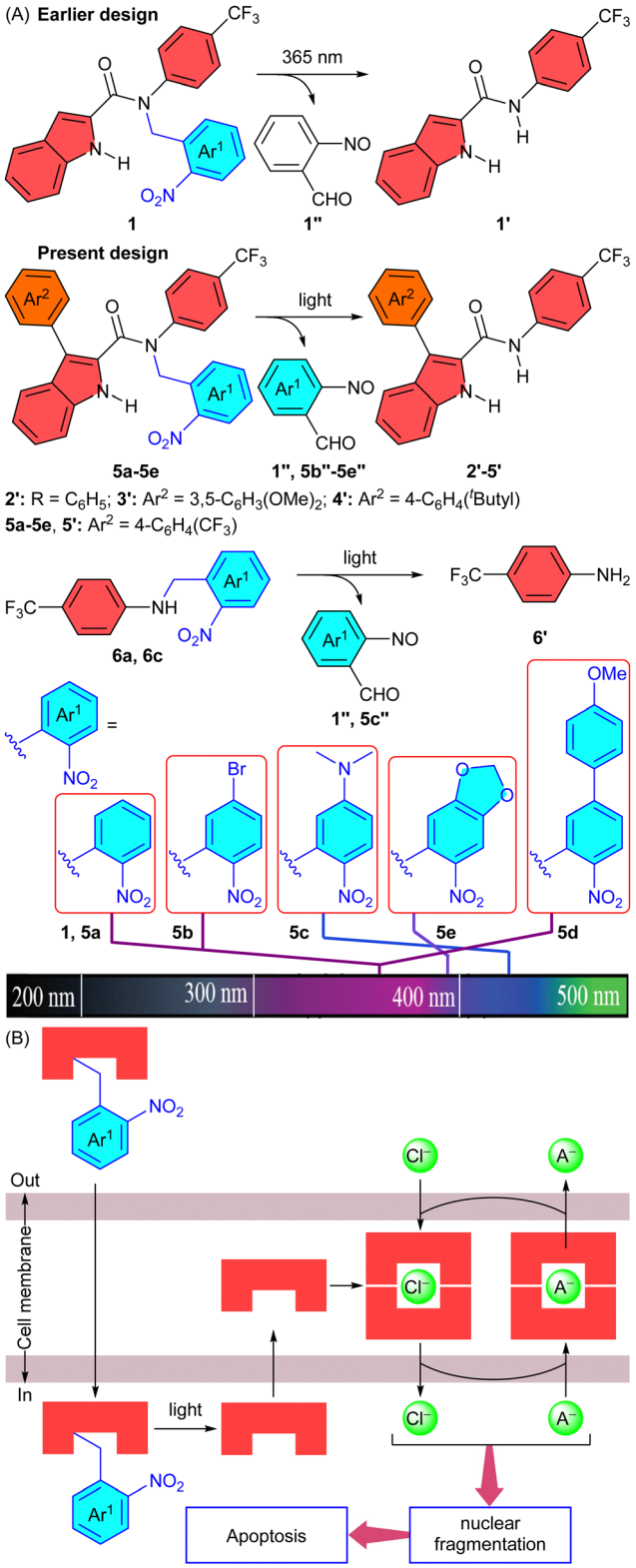

Fig. 1 Schematic representation of the earlier and present design of *o*-nitrobenzyl-linked indole-2-carboxamide-based photocleavable ion carriers showing chemical structures of procarriers **5a–5e**, active carriers **2′–5′** and amine-based control compounds **6a** and **6c** (A). Graphical representation of phototriggered release of an active anion carrier **2′–5′** from ONB-protected procarriers **5a–5c** to induce chloride-mediated apoptosis inside the cancer cells (B).

important targets because of their high degree of spatiotemporal control, remote addressability, and low cytotoxicity.[42] Light-responsive ionophores that have been studied include the use of either photoswitchable (*e.g.*, azobenzenes, acylhydrazones, phenylhydrazones, stilbenes, spiropyrans, *etc.*)[43–54] or photocleavable (*e.g.*, *o*-nitro aromatics)[55] groups. Photocages like *o*-nitrobenzyl (ONB) are versatile molecules that offer a way to generate a covalently linked active substrate with the help of external electromagnetic radiation,[56–58] and they have been used for either delivery[59–63] or activation[64–66] of anticancer drugs inside cancer cells. Recently, our group introduced an ONB-linked *N*-aryl-1*H*-indole-2-carboxamide system **1**, which was the first report of a photoactivable procarrier.[67] The procarrier would generate its active anion carrier form **1′** in the presence of external electromagnetic radiation inside the artificial liposomes and cancer cells (Fig. 1A), leading to recovery of ion transport ability and exhibiting cancer cell toxicity. The major limitation of this system was the use of harmful UV light (λ = 365 nm), which can lead to phototoxic cell damage or death following exposure,[68] for procarrier photoactivation. Ultraviolet light also has very limited cellular penetration, restricting its photouncaging ability to surface-level cells and/or tissue.[68] Thus, a shift to photocleavable groups activable in the visible region of the electromagnetic spectrum is necessary for the practical application of this system. Also, studies into the apoptotic mechanism of the active carrier were not conducted in the previous study as it was observed to precipitate in cell culture media, likely due to its less-than-optimum lipophilicity,[69] which necessitated an improvement in the design.

In our present design, we improved the lipophilicity of the active carriers by incorporating different aromatic moieties at position 3 of the indole ring to generate a set of modified active carriers **2′–5′** (Fig. 1A). The improved lipophilicity was expected to enhance their ion transport property as well as cytotoxicity. Secondly, in order to improve the photocleavable absorption wavelength of the procarriers, we modified the ONB photocleavable protecting group with different electron-donating groups to generate a set of modified procarriers **5a–5e** (Fig. 1A). The incorporation of electron-donating groups to the ONB group is well known to red-shift its absorption wavelength.[70,71] Thus, the incorporation of electron donating groups like *N*,*N*-dimethyl was expected to enhance the absorption wavelength of the procarrier and hence can be activated inside the cancer cells at higher wavelengths of electromagnetic radiation (Fig. 1B).

Results and discussion

Synthesis of active carriers 2′–5′

The overall synthesis of the designed transporters **2′–5′** is shown in Fig. 2A. In order to synthesize the active carriers **2′–5′**, 3-iodo-2-indole carboxylic acid **3**, which itself was synthesized from indole-2-carboxylic acid using the reported literature protocol,[72] was coupled with 4-trifluoromethyl aniline in the presence of EDC·HCl and HOBt to furnish the amide derivative **4**. Compound **4** was then coupled with different aryl boronic

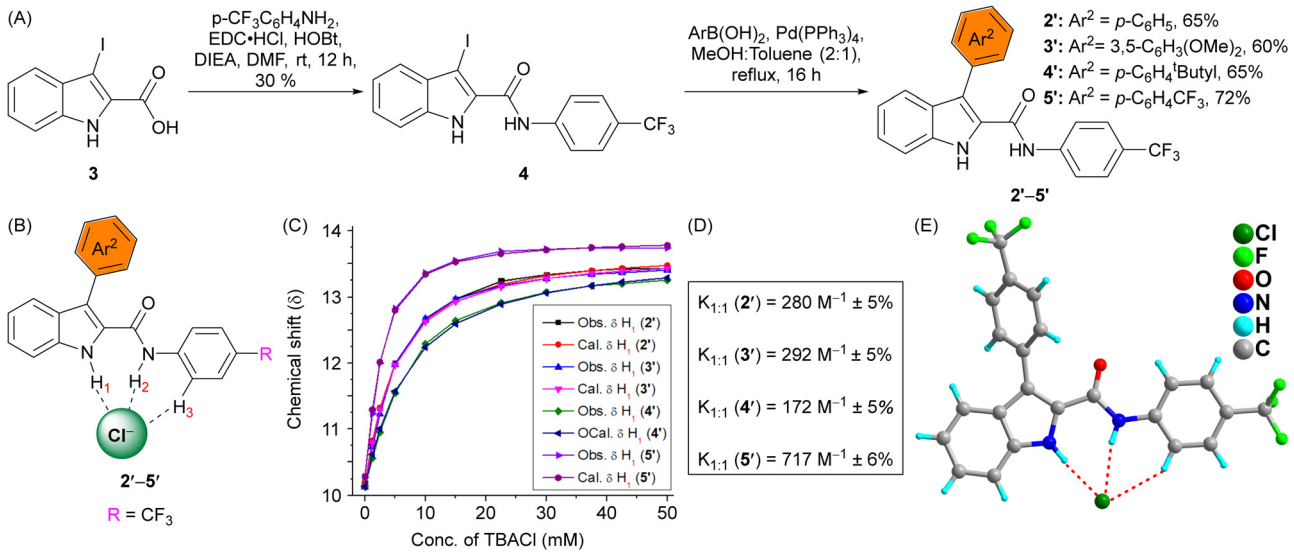

Fig. 2 Chemical synthesis of carriers **2′**–**5′** (A). Chemical structure of the carriers showing binding interactions with the chloride anion (B). The plot of chemical shifts (δ) of the H_1 proton *vs.* concentrations of TBACl added, fitted to a 1 : 1 binding model of BindFit for the active carriers **2′**–**5′** (C). Binding constant values of carriers **2′**–**5′**. (E) X-ray crystallographic structure of **5′** with the chloride anion (D).

acids using a Suzuki coupling reaction in the presence of $Pd(PPh_3)_4$ as the catalyst to synthesize the desired active carriers **2′**–**5′** in excellent yields.

The initial evidence of Cl^- binding by the receptors **2′**–**5′** was confirmed by performing the ^1H NMR titration studies in acetonitrile-d_3. Fresh samples of the receptors **2′**–**5′** were prepared in clean NMR tubes, and ^1H NMR for each sample was recorded. After that, tetrabutylammonium chloride (TBACl) was added to the samples in increasing equivalents, and the ^1H NMR spectrum was recorded after each addition. A significant downfield shift of (indole) N–H_1, (amide) N–H_2 and C_{Ar}–H_3 protons was observed, indicating the involvement of these protons in hydrogen bonding through (indole) N–$H_1\cdots Cl^-$, (amide) N–$H_2\cdots Cl^-$ and C_{Ar}–$H_3\cdots Cl^-$ non-covalent interactions (Fig. 2C and Fig. S1, S3, S5, S7, ESI†). Further analysis using the BindFit program[73] furnished a 1 : 1 (host : guest) binding stoichiometry with the association constant values ($K_{a(1:1)}/Cl^-$) of 717 ± 42 M^{-1} for **5′**, 280 ± 8 M^{-1} for **2′**, 292 ± 14 M^{-1} for **3′**, and 172 ± 10 M^{-1} for **4′**, respectively (Fig. 2D, Fig. S2, S4, S6, S8 and Table 1, ESI†), with the binding affinity sequence of **5′** > **3′** > **2′** > **4′**. The single-crystal X-ray diffraction analysis provided direct evidence of chloride binding to **5′** and revealed the formation of a **5′**·Cl^- complex in 1 : 1 binding mode (Fig. 2E). The chloride anion interacts with molecule **5′** through indole N–H_1, amide N–H_2 and C_{Ar}–H_3 hydrogen bonding interactions with a $H_1\cdots Cl^-$ distance of 2.18 Å, $H_2\cdots Cl^-$ distance of 2.34 Å, and $H_3\cdots Cl^-$ distance of 2.79 Å, respectively.

Ion transport studies

The anion recognition properties of the active compounds **2′**–**5′** prompted us to evaluate their ion transport properties across large unilamellar vesicles (LUVs). In order to do that, vesicles entrapping 8-hydroxypyrene-1,3,6-trisulfonate (HPTS, pK_a = 7.2) dye were prepared from egg-yolk phosphatidylcholine (EYPC) lipid to get EYPC-LUVs⊃HPTS[74] (see ESI†). After that, a pH gradient, ΔpH = 0.8 (pH_{in} = 7.0 and pH_{out} = 7.8), was created across the vesicular membrane by adding NaOH into the extravesicular buffer. The dissipation of pH gradient upon the addition of compounds **2′**–**5′** and the previously reported active compound **1′** was monitored by measuring the fluorescence intensity of HPTS at λ_{em} = 510 nm (λ_{ex} = 450 nm). Eventually, the vesicles were lysed by adding Triton X-100 to get the maximum fluorescence intensity. The comparison of ion transport activity at a concentration of 0.2 μM provided the activity sequence: **5′** > **3′** > **2′** > **1′** > **4′**, respectively (Fig. 3A). The Hill analysis of the dose–response plots of the compounds **2′**, **3′**, **5′** and **1′** provided the EC_{50} values of 0.132 ± 0.015 μM (compound-to-lipid ratio = 0.00194), 0.113 ± 0.012 μM (compound-to-lipid ratio = 0.00167), 0.051 ± 0.008 μM (compound-to-lipid ratio = 0.00075), and 0.184 ± 0.018 μM (compound-to-lipid ratio = 0.00271), respectively (Fig. S10–S12, S14 and Table 1, ESI†). The Hill coefficient (n) of the compounds was ∼2, which indicates that two receptor molecules are involved in forming the active transport system during the ion transport process. The Hill analysis could not be evaluated

Table 1 Summary of pK_a (indole-N-H_1), log P, chloride association constant K_a (M^{-1}) recorded in acetonitrile-d_3, EC_{50} (μM), and Hill coefficient values of compounds **2′**–**5′** and **1′**

Comp.	log P^a	$pK_a{}^a$	$K_a{}^b$ (M^{-1})/Cl^-	EC_{50} (μM)	n
1[67]	3.96	11.76	599 ± 13	0.184 ± 0.018	2.7 ± 0.3
2′	5.61	15.80	280 ± 8	0.132 ± 0.015	2.2 ± 0.4
3′	5.29	11.68	292 ± 14	0.113 ± 0.012	2.6 ± 0.4
4′	7.15	11.84	172 ± 10	—[c]	—[c]
5′	6.49	11.81	717 ± 42	0.051 ± 0.008	2.1 ± 0.3

[a] Calculator plugins of the MarvinSketch program were used for calculating log P and pK_a values. [b] Association constants were obtained based on the 1 : 1 binding model for N–H protons. [c] Could not be determined due to the precipitation of the compound at higher concentrations.

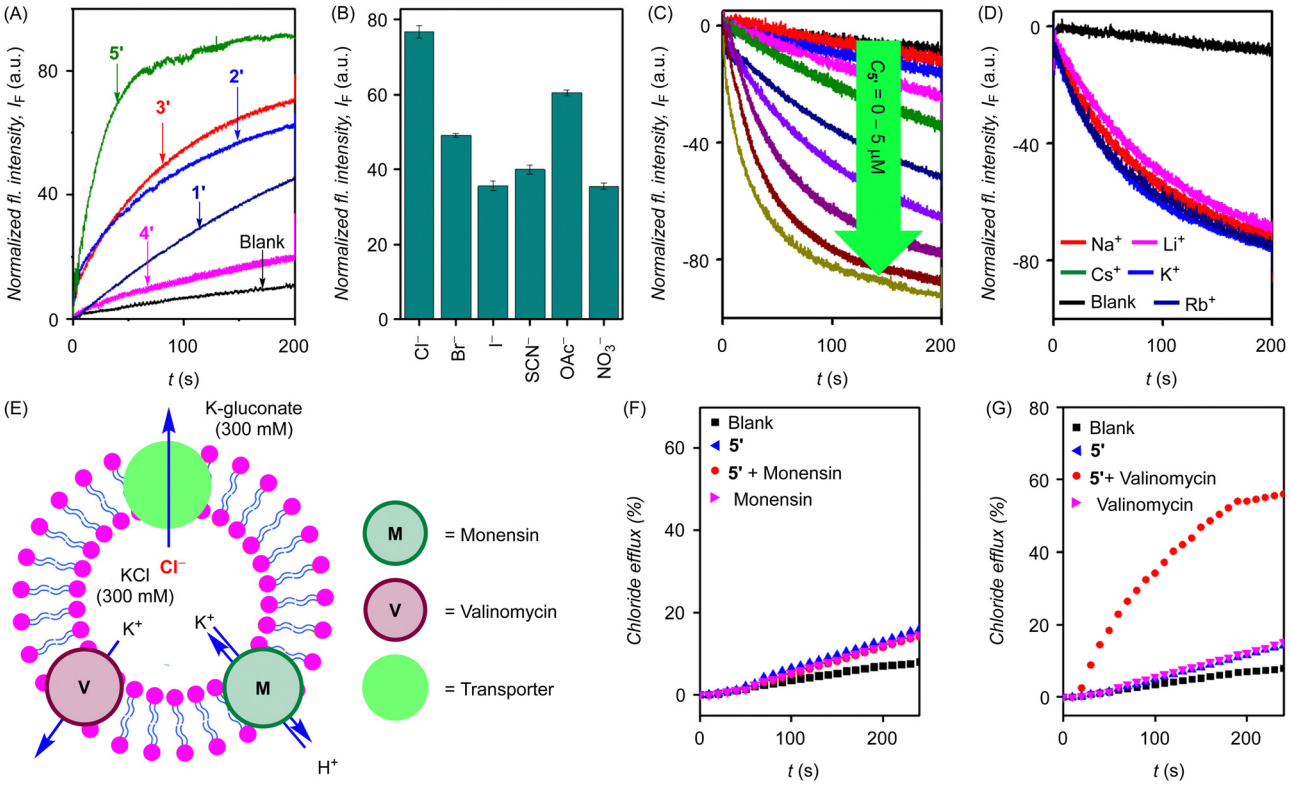

Fig. 3 Activity comparison of **2′–5′** and **1′** (0.2 μM each) across EYPC-LUVs⊃HPTS (A). Anion selectivity of **5′** (0.2 μM) by varying external anions across EYPC-LUVs⊃HPTS; each bar graph represents mean ion transport activity, calculated from three independent experiments (B). Concentration-dependent activity of compound **5′** across EYPC-LUVs⊃lucigenin (C). Cation selectivity of **5′** (0.7 μM) by varying external anions across EYPC-LUVs⊃lucigenin (D). Schematic representation of ISE-based valinomycin and monensin assay (E). Normalized chloride efflux of **5′** in the presence and absence of monensin (F), and the presence and absence of valinomycin (G).

for **4′** due to its precipitation observed at higher concentrations in the buffer (Fig. S13, ESI†). The compounds **2′**, **3′**, and **5′** showed better ion transport activity than **1′**, with **5′** showing almost 4-fold enhancement in the ion transport activity compared to **1′**. The incorporation of an aromatic moiety to the indole ring increases the hydrophobicity of the carriers, which in turn increases the membrane permeability and eventually enhances the ion transport activity. Among the modified anionophores **2′–5′**, **5′** showed better transport activity, likely due to two CF_3 groups, which are known to increase the membrane permeability and binding affinity of the ionophores.

Chloride leakage studies

In order to check the transport of Cl^- ions, the transport activity of the highest active compound in the HPTS assay **5′** was monitored across EYPC-LUVs⊃lucigenin.[75] Vesicles were prepared by entrapping the lucigenin dye and $NaNO_3$ salt, and subsequently, a Cl^-/NO_3^- gradient was created across the vesicular membrane by adding NaCl in the extravesicular buffer solution. The transport of Cl^- by **5′** ions was measured by monitoring the fluorescence intensity of intravesicular lucigenin dye at λ_{em} = 535 nm (λ_{ex} = 455 nm). A significant decrease in the fluorescence intensity of the lucigenin dye was observed upon the addition of carrier **5′**. The dose-dependent chloride transport activity of **5′** is shown in Fig. 3C. The Hill analysis provided the EC_{50} value of 0.870 ± 0.065 μM and n value of ~2, indicating the involvement of two receptor molecules in catalyzing the ion transport process (Fig. S18, ESI†). Furthermore, the variation of external cations by using different M^+/Cl^- salts (where, M^+ = Li^+, Na^+, K^+, Rb^+, and Cs^+) in the external buffer did not have any significant effect on the ion transport rate of **5′** (Fig. 3D), and hence, once again rules out any active role of cations in the ion transport process as was observed while changing the external cations in the above HPTS studies.

Ion selectivity and mechanism of ion transport

Mechanistically, the disruption of the pH gradient across EYPC-LUVs⊃HPTS based vesicles can occur through the following different modes: (a) H^+/X^- symport, (b) OH^-/X^- antiport, (c) H^+/M^+ antiport, or (d) OH^-/M^+ symport. In order to get insight into the possible mechanistic route among the above different possible ways, the ion transport activity of **5′** was monitored across EYPC-LUVs⊃HPTS using intracellular NaCl and an iso-osmolar extravesicular M^+/Cl^- salt (where M^+ = Li^+, Na^+, K^+, Rb^+, and Cs^+). Changing the extravesicular cations did not provide any significant change in the ion transport activity of

the 5′ (Fig. S16, ESI†) and hence, suggests that H^+/M^+ antiport and OH^-/M^+ symport mechanisms did not operate in the ion transport process.[76] However, changing the extravesicular Na^+/X^- salt (X^- = Cl^-, Br^-, I^-, SCN^-, OAc^-, and NO_3^-) made a significant change in the ion transport activity (Fig. 3B), indicating the role of anions in an overall transport process, and hence indicates that the ion transport process can occur through either OH^-/X^- antiport or H^+/X^- symport mode.

The anion antiport process was confirmed through chloride-based ion-selective electrode (ISE) studies. Vesicles were prepared by entrapping with KCl (300 mM) and suspended in potassium gluconate solution (300 mM, Fig. 3E). The Cl^- efflux using a chloride sensitive ion selective electrode (ISE) was monitored in the presence and absence of valinomycin (a highly selective K^+ carrier) and monensin (an H^+/K^+ antiporter). No noticeable change was observed in the Cl^- efflux by 5′ in the presence of monensin (Fig. 3F), but, on the other hand, a significant increase in the Cl^- efflux by 5′ was observed in the presence of valinomycin (Fig. 3G). The synergistic cooperative effect of the valinomycin with the anionophore 5′ indicates the occurrence of an electrogenic mode of ion transport and, thus, validates the operation of an anion antiport mechanism for the ion transport process.[77–79]

Additionally, the evidence of the carrier mode of ion transport by 5′ was obtained by performing the classic U-tube experiment.[17,80–82] Significant chloride transport was observed from one of the arms of the U-tube (source arm, containing 500 mM NaCl) to the other arm (receiver arm, containing 500 mM $NaNO_3$) using a chloride ion selective electrode (Fig. S23, ESI†).

Synthesis of caged procarriers 5a–5e

Compound 5′, with the optimum anion binding and transport capabilities, was selected for caging with different ONB-based cages. In order to synthesize the ONB-protected compounds **5a–5e** based on the free compound 5′, initially, the ONB-based amine compounds **6a–6e** were synthesized by coupling 4-trifluoromethyl aniline 6′ with different nitrobenzaldehyde compounds **10a–10e**. This reaction was done in two steps: (i) coupling of nitrobenzaldehyde derivatives **10a–10e** with 4-trifluoromethylaniline 6′ in dichloromethane under reflux conditions in the presence of pyrrolidine as a catalyst and 3–4 Å molecular sieves to give the imine intermediates; (ii) *in situ* reduction of imine compounds using sodium borohydride in methanol to furnish the desired amines **6a–6e**. Meanwhile, 3-iodo-2-indolecarboxylate **13** was coupled with 4-trifluoromethylphenyl boronic acid following a Suzuki coupling condition in the presence of $Pd(PPh_3)_4$ as the catalyst to obtain methyl 3-(4-(trifluoromethyl)phenyl)-1*H*-indole-2-carboxylate **14**. This ester-based compound **14** was subsequently hydrolyzed using aqueous sodium hydroxide in a 1 : 1 mixture of methanol and tetrahydrofuran for 24 h at r.t. to get the acid derivative **15**. Finally, acid **15** was coupled with different amines

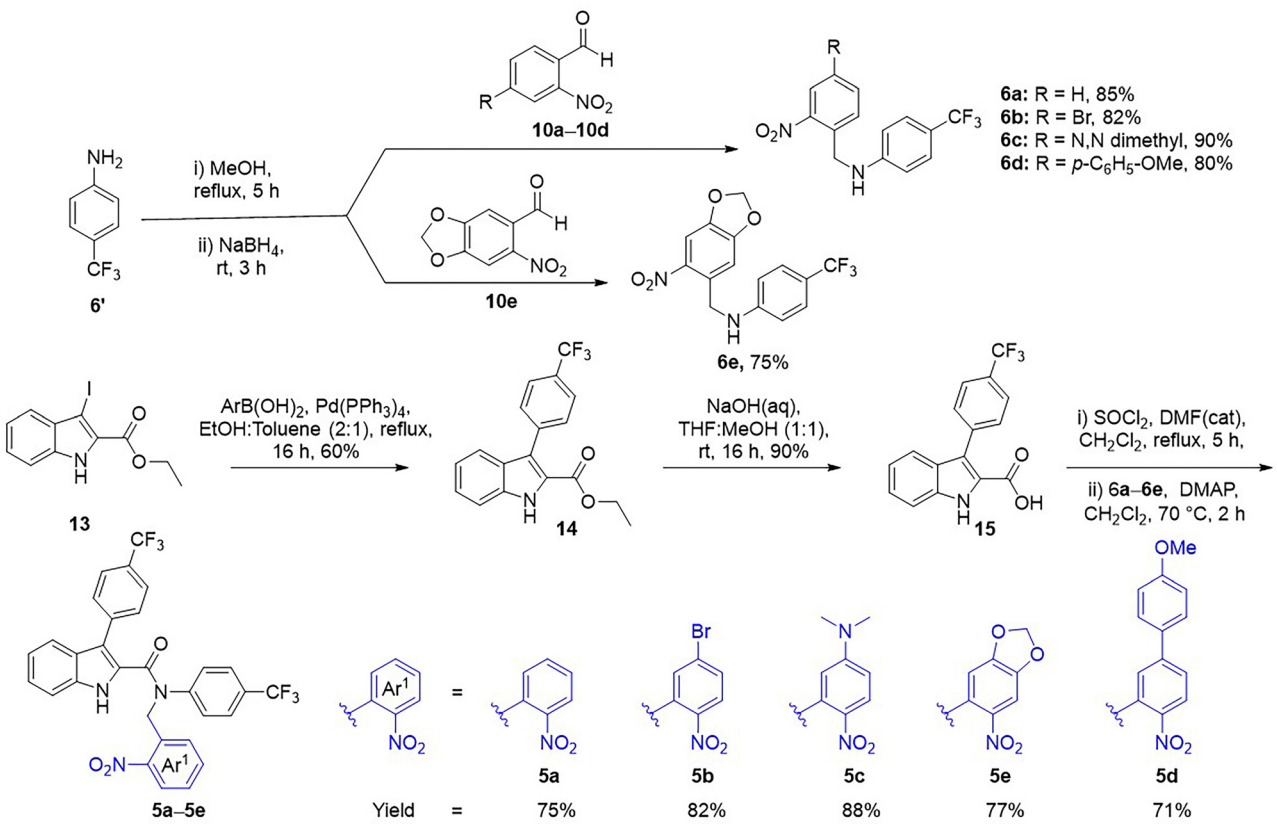

Fig. 4 Chemical synthesis of caged procarriers **5a–5d**.

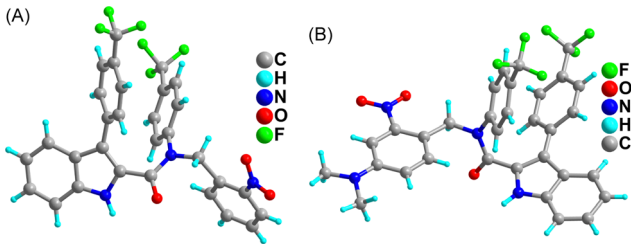

Fig. 5 X-ray crystal structures of caged procarriers **5a** (A) and **5c** (B), respectively.

6a–6e in dichloromethane under reflux conditions using triethylamine as the base to furnish the desired ONB-protected compounds **5a–5e** in 71–88% yield (Fig. 4). Crystal structures of **5a**, **5c** and **5d** were determined through single crystal X-ray diffraction (Fig. 5 and Fig. S44–S46, ESI†).

Photoresponsive studies

Initially, the UV-vis absorption studies of the ONB-protected compounds **5a–5e** were performed in acetonitrile. The UV-vis absorption spectra of the compounds are shown in Fig. 6A. The absorption spectra of **5a**, **5b**, **5d**, and **5e** displayed λ_{max} centered around 310 nm with the absorbance peaks of **5a**, **5b**, and **5e** extending up to the wavelength of 385 nm, whereas **5d** up to 408 nm. On the other hand, the absorption spectra of **5c** displayed λ_{max} at 410 nm, and the absorbance peak extended up to 500 nm. Moreover, the UV-vis absorption spectrum of **5c** does not change much upon changing the pH from 6–8 (Fig. S24, ESI†). The wavelength of the external source required to photolyze these compounds was determined based on these spectra, and compound **5c** was expected to photolyze at a longer wavelength compared to the other derivatives. Thus, the photocleavage studies for all the protected compounds **5a–5e** were performed at 400 nm using LEDs as the external source of light, and studies for **5c** were also performed at 450 nm. All these studies were conducted using ^{1}H NMR, where the ^{1}H NMR spectra of solutions of **5a–5e** DMSO-d_6 were recorded following photoirradiation under 400 nm (using a 12 W LED) at different time intervals. Comparison of the procarrier spectra before and after photoirradiation with the non-protected carrier **5′** indicated efficient photocleavage properties, generating the active compound **5′** and the corresponding *o*-nitrosobenzaldehyde byproduct (Fig. S25–S29, ESI†). The NMR-based photoirradiation study of **5c** at 450 nm was also performed and efficient photolysis was confirmed (Fig. 6B). The photocleavage study of **5c** under 450 nm light was also performed using HRMS. A solution of **5c** (10 mM) in methanol : acetonitrile : water (2 : 2 : 1) mixture was photoirradiated at 450 nm for 2 h (3 × 1 W LEDs). The mass spectroscopic data provided peaks at m/z = 449.1090 and 179.0821, corresponding to **5′** and 4-dimethylamino-2-nitrosobenzaldehyde **5c″** byproduct in the solution (Fig. S32, ESI†).

Phototriggered ion transport studies

After successful photolytic studies of **5a–5e**, the compounds were subjected to phototriggered ion transport studies across EYPC-LUVs ⊃ HPTS.[83] Vesicles containing **5a–5e** (0.2 mM) were photoirradiated at 400 nm and 450 nm for different time intervals, and the ion transport activity was monitored at each time point. The transport activities were compared by setting the ion transport activity of the blank sample as 0, and that of active compound **5′** as 100%. The non-photoirradiated samples of **5a–5e** did not show any activity at the concentrations studied. Efficient photoactivation was achieved upon photoirradiation at 400 nm for all procarriers (Fig. S34A–S38A, ESI†). They exhibited no activity on irradiation at 450 nm while significant activation was achieved for procarrier **5c** on irradiation under 450 nm (Fig. 6D) while procarriers **5a**, **5b**, **5c**, and **5d** were inactive (Fig. S34B–S38B, ESI†) following 450 nm irradiation. Moreover, photoirradiation of EYPC-LUVs ⊃ HPTS treated with 1% DMSO for five minutes did not yield any change in fluorescence readout following the base pulse, indicating that the photoirradiation does not disrupt the integrity of the vesicles. The increment in the activity of **5a–5e** upon photoirradiation at different wavelengths indicates the photocleavage of procarriers inside the lipid vesicles generating the active compound **5′**, which drives the ion transport across the lipid bilayer membrane.

Geometry optimization and binding energy calculation

To obtain the possible geometry of the $[(\mathbf{5}')_2 + Cl^-]$ complex, which was chosen based on the experimentally determined Hill coefficient value of $n \sim 2$ and Cl^- selectivity, density functional theory (DFT) calculation studies were performed. The initial coordinates for the calculations were obtained by using the CONFLEX 8 software program,[84,85] which gave several conformational structures with similar populations (Fig. S48, ESI†). Subsequently, the structure with the highest Boltzmann population was taken for further geometry optimization by the Gaussian 09 program[86] using the B3LYP functional and 6-31G(d,p) basis set.[87] The geometry optimized structure of the $[(\mathbf{5}')_2 + Cl^-]$ complex showed that the two receptor molecules involved in the binding of a Cl^- are oriented orthogonally to each other for proper binding of the chloride ion (Fig. 6E). The structure confirmed that each receptor participates in chloride recognition through indole-N–$H_1\cdots Cl^-$ ($H_1\cdots Cl^-$ = 2.42 Å), amide-N–$H_2\cdots Cl^-$ ($H_2\cdots Cl^-$ = 2.42 Å) and C_{Ar}–$H_3\cdots Cl^-$ ($H_3\cdots Cl^-$ = 2.80 Å), hydrogen bonding interactions. Furthermore, the binding energy of −47.89 kcal mol^{-1} was calculated for the $[(\mathbf{5}')_2 + Cl^-]$ complex (see ESI†).

Ion carrier activity in the cancer cell line

The most efficient ion carrier **5′** was chosen for testing in the MCF-7 human breast cancer cell line. MCF-7 cells grown in DMEM were treated with **5′** in a dose range of 0–20 μM for 24 h, following which the cell viability was assessed using MTT dye, which yielded an IC_{50} value of 6.02 μM (Fig. S39, ESI†). The cell death observed upon treatment with the carrier resulted from the ion transport induced disruption of the chloride ion gradient across the cell membrane, which in turn triggers the cellular apoptotic pathway. Verification of this chloride ion transport by **5′** was conducted through the MQAE assay.[16,88]

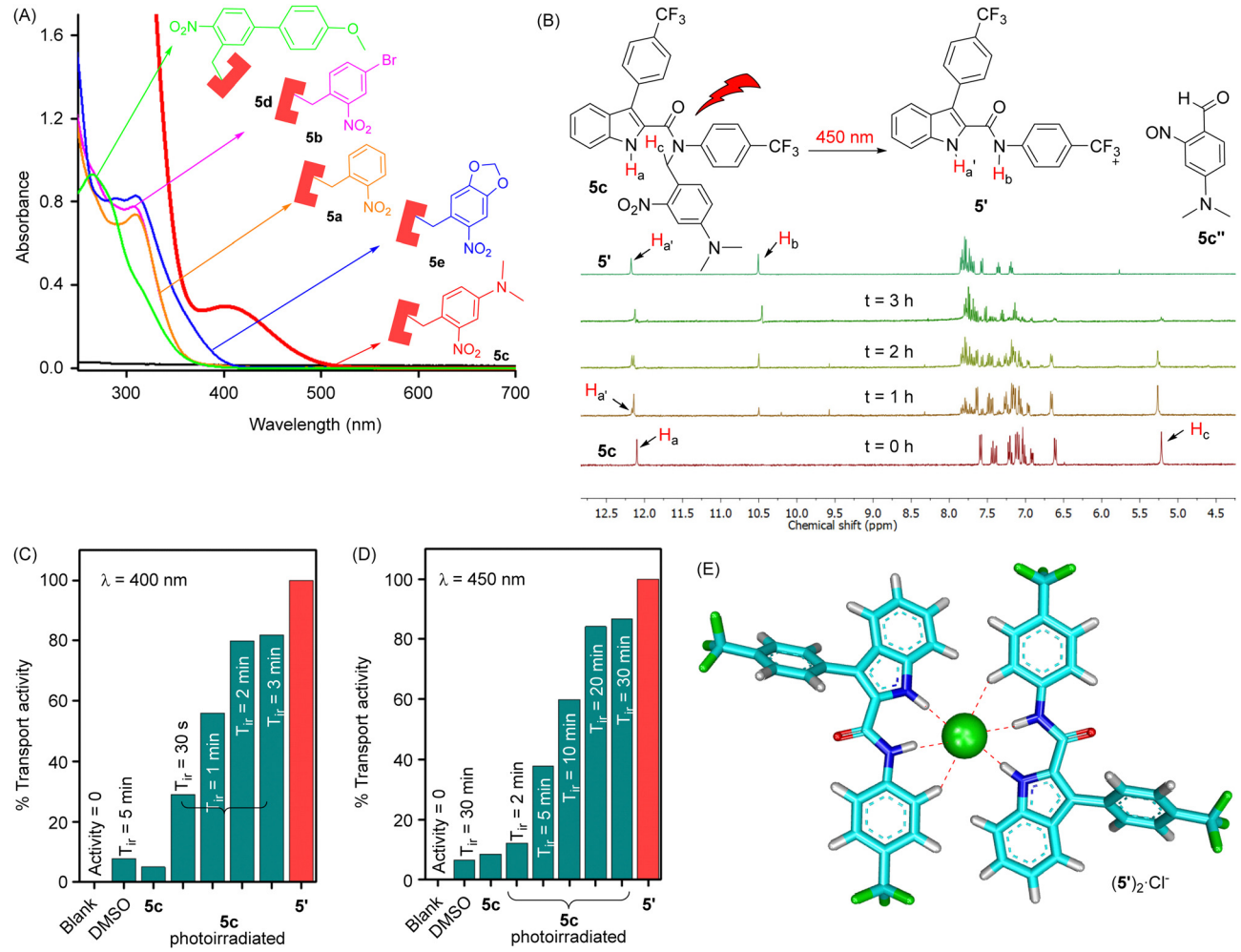

Fig. 6 UV-visible absorption spectrum of *o*-NB protected procarrier compounds **5a–5e** (A). Phototriggered release of an active carrier **5′** from ONB-protected procarrier **5c** monitored by ^{1}H NMR studies recorded in DMSO-d_6 photoirradiated using 450 nm LEDs at different intervals of time (B). Normalized ion transport activity data of **5c** upon photoirradiation at 400 nm (C), and 450 nm (D), respectively. The geometry-optimized structure of the [(**5′**)$_2$ + Cl$^-$] complex (E).

N-(Ethoxycarbonylmethyl)-6-methoxyquinolinium bromide (MQAE) is a cell permeable fluorescent dye that undergoes collisional quenching in the presence of a chloride ion.[89,90] Carrier 5′ at 5, 10, and 25 μM concentrations was added to

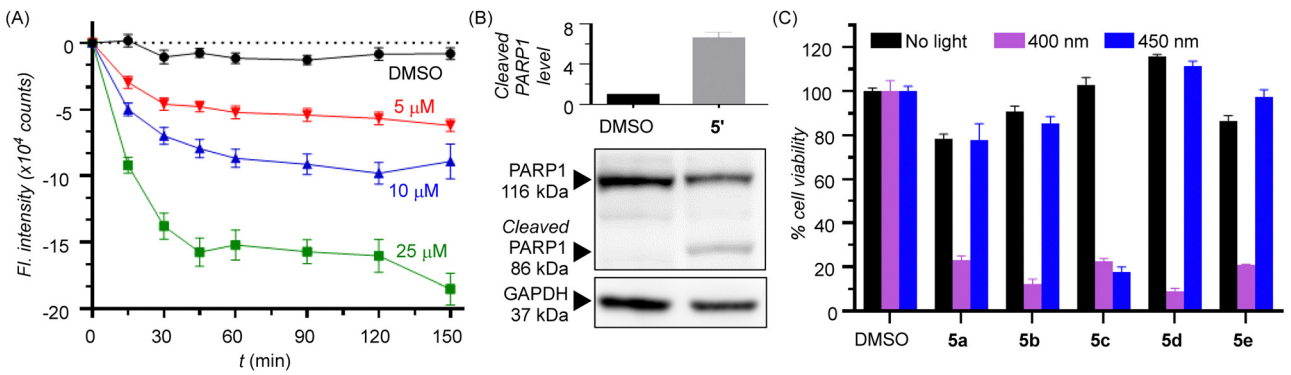

Fig. 7 Time dependent change in fluorescence signal intensity in MQAE pretreated MCF-7 cells following addition of carrier **5′** (0–25 μM) (A). An increased rate of fluorescence quenching was observed with an increasing dosage of **5′**, indicating a higher rate of chloride influx in the cells. Immunoblot analysis of PARP1 cleavage in MCF-7 cells treated with **5′** (B). Protein expression level was quantified with respect to GAPDH. The plot of cleaved PARP1 level indicates the fold change in expression relative to the DMSO-treated control (*Y*-axis). Cell viability observed in MCF-7 cells on treatment with procarriers **5a–5e** (10 μM) for 24 h both in the absence of light (black) and upon photoirradiation at 400 nm (20 min, violet) and 450 nm (2 h, blue) using LEDs (C).

MCF-7 cells pretreated with MQAE and the fluorescence intensity (λ_{ex} = 350 nm, λ_{em} = 460 nm) was monitored over time. An increased rate of fluorescence quenching with time was observed with an increasing dosage of **5′** (Fig. 7A), confirming carrier-facilitated influx of Cl^- into the cell. During the apoptotic process, the poly(ADP-ribose) polymerase-1 (PARP1) DNA repair protein gets cleaved by exogenous caspases to prevent futile DNA repair.[91–94] Thus, induction of apoptotic cell death by the carrier was verified by probing for PARP1 cleavage. Expression of cleaved PARP1 was observed on immunoblot analysis of cells treated with 5 μM of carrier **5′** (Fig. 7B), confirming apoptosis induction. Glyceraldehyde 3-phosphate dehydrogenase (GAPDH) was used as the loading control for quantification of expression levels of PARP1 (Fig. 7B).

Phototriggered anticancer activity

Assessment of cytotoxicity of the procarriers was conducted in MCF-7 cells at 10 μM concentration. Prior to photoactivation, compounds **5b–5e** exhibited negligible cytotoxicity, while **5a** exhibited moderate toxicity at the tested concentrations. Procarrier activation in MCF-7 cultures was assessed under light of 400 nm (violet) and 450 nm (blue) wavelengths. Cultures treated with **5a–5e** on irradiation under 400 nm light for 20 min exhibited significant cell death (Fig. 7C), indicating successful photoactivation of all procarrier systems and the subsequent disruption of cellular chloride homeostasis by the released active carrier **5′**. For cultures irradiated under 450 nm light (2 h), toxicity was observed only in cells treated with **5c** (Fig. 7C). This was in line with our previous observations where only **5c**, which had an absorption peak in the blue region, was capable of ion transport on activation under 450 nm light. The other procarriers **5a**, **5b**, **5d**, and **5e** do not undergo substantial photocleavage at this wavelength and thus do not show a significant increase in cytotoxicity. Compounds **6a–6e** were used as photocleavage controls that would release the *o*-nitrosoaldehyde byproducts on photocleavage along with the non-toxic 4-trifluoromethylaniline on photoactivation (photouncaging of **6a** with 400 nm and **6c** with 450 nm is shown in Fig. S30 and S31, ESI†). All controls exhibited negligible toxicity on activation under 400 nm light (for 20 min), indicating that the byproducts do not contribute to cell death on procarrier photoactivation (Fig. S40, ESI†). Control **6c** also exhibited negligible cytotoxicity on irradiation under 450 nm light for 2 h (Fig. S41, ESI†).

Conclusions

In conclusion, we have successfully modified the previously studied indole-2-carboxamide ion carrier **1′** by incorporating different aromatic moieties to generate the new set of ion carriers **2′–5′** with efficient ion transport activities. The highest active compound **5′** showed an almost four-fold increment in the transport activity as compared to the previously studied **1′**. The chloride binding studies were confirmed by ^{1}H NMR titration studies, and the direct proof of chloride binding of **5′** was obtained by solid-state X-ray crystallographic studies. The highest active compound **5′**, furnished the EC_{50} value of 0.05 μM with a Hill coefficient n value of ~2, indicating the involvement of two receptors in the formation of an active ion transport system to drive the ion transport across the membrane. Detailed mechanistic studies of ion transport confirmed the operation of an anion antiport mechanism. The actively transported **5′** showed efficient cytotoxicity inside the MCF-7 breast cancer cells, which was shown to be the result of carrier-induced chloride influx that triggered apoptosis. Eventually, all the synthesized procarriers were photoactivated inside the MCF-7 cancer cells at 400 nm of electromagnetic radiation, and the corresponding *N*,*N*-dimethyl-based procarrier was photoactivated at 450 nm. This photoactivation at the higher wavelengths of the electromagnetic spectrum is highly desirable for its practical biological applications.

Author contributions

M. A. and P. T. conceived the project. M. A., P. T. and M. L. directed the research plans. M. A. synthesized and characterized the compounds, and performed the ion transport studies and photoactivation studies. N. J. R. performed the biological studies. D. M. performed the computational studies. T. V. performed the X-ray crystallographic analysis of the compounds. M. A. and N. J. R. wrote the paper. P. T. and M. L. reviewed the paper. All authors have approved the final version of the manuscript.

Data availability

The data supporting this article have been included as part of the ESI.† Crystallographic data have been deposited at the Cambridge Crystallographic Data Centre (CCDC) with IDs 2127603 for **5′**, 2127604 for **5′**·Cl^-, 2155430 for **5a**, 2127605 for **5c**, 2127606 for **5d**, and 2127607 for **6e**, and can be obtained from **https://www.ccdc.cam.ac.uk/structures/**.

Conflicts of interest

There are no conflicts to declare.

Acknowledgements

This work was supported by the Science and Engineering Research Board, Government of India (grant no. CRG/2022/001640) and Indian Institute of Science Education and Research Pune. MA and DM thank UGC, Govt. of India, for the research fellowships. NJR thanks CSIR, Government of India, for the research fellowship. We thank Prof. Lalu V. (College of Engineering Trivandrum) and Dr Abhijith K. (IISER Pune) for their valuable inputs and discussions.

Notes and references

1 M. L. Davila, *Curr. Opin. Gastroen.*, 2006, **22**, 44–47.

2 D. J. Franklin and L. Packel, *Arch. Phys. Med. Rehabil.*, 2006, **87**, 91–93.
3 M. Brydøy, S. D. Fosså, O. Dahl and T. Bjøro, *Acta Oncol.*, 2007, **46**, 480–489.
4 M. Ogawa, *Nihon Rinsho*, 1997, **55**, 1017–1023.
5 M. Montaño-Samaniego, D. M. Bravo-Estupiñan, O. Méndez-Guerrero, E. Alarcón-Hernández and M. Ibáñez-Hernández, *Front. Oncol.*, 2020, **10**, 605380.
6 W. R. Sellers and D. E. Fisher, *J. Clin. Invest.*, 1999, **104**, 1655–1661.
7 J. M. Brown and L. D. Attardi, *Nat. Rev. Cancer*, 2005, **5**, 231–237.
8 L. Portt, G. Norman, C. Clapp, M. Greenwood and M. T. Greenwood, *Biochim. Biophys. Acta*, 2011, **1813**, 238–259.
9 R. S. Y. Wong, *Clin. Cancer Res.*, 2011, **30**, 87.
10 J. M. Lee, F. M. Davis, S. J. Roberts-Thomson and G. R. Monteith, *Am. J. Physiol.: Cell Physiol.*, 2011, **301**, C969–C976.
11 R. S. Frey and A. B. Malik, *Am. J. Physiol.: Lung Cell. Mol. Physiol.*, 2004, **2**(286), L1–L3.
12 L. Yu, X. H. Jiang, Z. Zhou, L. L. Tsang, M. K. Yu, Y. W. Chung, X. H. Zhang, A. M. Wang, H. Tang and H. C. Chan, *PLoS One*, 2011, **6**, e17322–e17322.
13 M. D. Davis, J. J. Clemens, T. L. Macdonald and K. R. Lynch, *J. Biol. Chem.*, 2005, **280**, 9833–9841.
14 R. Pérez-Tomás, B. Montaner, E. Llagostera and V. Soto-Cerrato, *Biochem. Pharmacol.*, 2003, **66**, 1447–1452.
15 P. Manuel-Manresa, L. Korrodi-Gregório, E. Hernando, A. Villanueva, D. Martínez-García, A. M. Rodilla, R. Ramos, M. Fardilha, J. Moya, R. Quesada, V. Soto-Cerrato and R. Pérez-Tomás, *Mol. Cancer Ther.*, 2017, **16**, 1224–1235.
16 S.-K. Ko, S. K. Kim, A. Share, V. M. Lynch, J. Park, W. Namkung, W. Van Rossom, N. Busschaert, P. A. Gale, J. L. Sessler and I. Shin, *Nat. Chem.*, 2014, **6**, 885.
17 N. Busschaert, M. Wenzel, M. E. Light, P. Iglesias-Hernández, R. Pérez-Tomás and P. A. Gale, *J. Am. Chem. Soc.*, 2011, **133**, 14136–14148.
18 S. J. Moore, C. J. E. Haynes, J. González, J. L. Sutton, S. J. Brooks, M. E. Light, J. Herniman, G. J. Langley, V. Soto-Cerrato, R. Pérez-Tomás, I. Marques, P. J. Costa, V. Félix and P. A. Gale, *Chem. Sci.*, 2013, **4**, 103–117.
19 T. Saha, M. S. Hossain, D. Saha, M. Lahiri and P. Talukdar, *J. Am. Chem. Soc.*, 2016, **138**, 7558–7567.
20 N. Busschaert, S.-H. Park, K.-H. Baek, Y. P. Choi, J. Park, E. N. W. Howe, J. R. Hiscock, L. E. Karagiannidis, I. Marques, V. Félix, W. Namkung, J. L. Sessler, P. A. Gale and I. Shin, *Nat. Chem.*, 2017, **9**, 667–675.
21 E. N. W. Howe, N. Busschaert, X. Wu, S. N. Berry, J. Ho, M. E. Light, D. D. Czech, H. A. Klein, J. A. Kitchen and P. A. Gale, *J. Am. Chem. Soc.*, 2016, **138**, 8301–8308.
22 N. Busschaert, R. B. P. Elmes, D. D. Czech, X. Wu, I. L. Kirby, E. M. Peck, K. D. Hendzel, S. K. Shaw, B. Chan, B. D. Smith, K. A. Jolliffe and P. A. Gale, *Chem. Sci.*, 2014, **5**, 3617–3626.
23 A. Roy, O. Biswas and P. Talukdar, *Chem. Commun.*, 2017, **53**, 3122–3125.
24 S. V. Shinde and P. Talukdar, *Org. Biomol. Chem.*, 2019, **17**, 4483–4490.
25 S. V. Shinde and P. Talukdar, *Angew. Chem., Int. Ed.*, 2017, **56**, 4238–4242.
26 Y. R. Choi, B. Lee, J. Park, W. Namkung and K.-S. Jeong, *J. Am. Chem. Soc.*, 2016, **138**, 15319–15322.
27 M. M. Tedesco, B. Ghebremariam, N. Sakai and S. Matile, *Angew. Chem., Int. Ed.*, 1999, **38**, 540–543.
28 P. Talukdar, G. Bollot, J. Mareda, N. Sakai and S. Matile, *Chem. – Eur. J.*, 2005, **11**, 6525–6532.
29 T. Kiwada, K. Sonomura, Y. Sugiura, K. Asami and S. Futaki, *J. Am. Chem. Soc.*, 2006, **128**, 6010–6011.
30 G. A. Woolley and B. A. Wallace, *Biochemistry*, 1993, **32**, 9819–9825.
31 L. Lien, D. C. J. Jaikaran, Z. Zhang and G. A. Woolley, *J. Am. Chem. Soc.*, 1996, **118**, 12222–12223.
32 Y. Kobuke, K. Ueda and M. Sokabe, *J. Am. Chem. Soc.*, 1992, **114**, 7618–7622.
33 W. Si, Z.-T. Li and J.-L. Hou, *Angew. Chem., Int. Ed.*, 2014, **53**, 4578–4581.
34 M. Fares, X. Wu, D. Ramesh, W. Lewis, P. A. Keller, E. N. W. Howe, R. Pérez-Tomás and P. A. Gale, *Angew. Chem., Int. Ed.*, 2020, **59**, 17614–17621.
35 N. Akhtar, N. Pradhan, A. Saha, V. Kumar, O. Biswas, S. Dey, M. Shah, S. Kumar and D. Manna, *Chem. Commun.*, 2019, **55**, 8482–8485.
36 I. F. Tannock and D. Rotin, *Cancer Res.*, 1989, **49**, 4373–4384.
37 W. Van Rossom, D. J. Asby, A. Tavassoli and P. A. Gale, *Org. Biomol. Chem.*, 2016, **14**, 2645–2650.
38 N. Busschaert, C. Caltagirone, W. Van Rossom and P. A. Gale, *Chem. Rev.*, 2015, **115**, 8038–8155.
39 J. A. Malla, R. M. Umesh, S. Yousf, S. Mane, S. Sharma, M. Lahiri and P. Talukdar, *Angew. Chem., Int. Ed.*, 2020, **59**, 7944–7952.
40 A. Mondal, J. A. Malla, H. Paithankar, S. Sharma, J. Chugh and P. Talukdar, *Org. Lett.*, 2021, **23**, 6131–6136.
41 J. A. Malla, V. K. Sharma, M. Lahiri and P. Talukdar, *Chem. – Eur. J.*, 2020, **26**, 11910.
42 M. R. Banghart, M. Volgraf and D. Trauner, *Biochemistry*, 2006, **45**, 15129–15141.
43 R. F. Khairutdinov and J. K. Hurst, *Langmuir*, 2004, **20**, 1781–1785.
44 M. Ahmad, S. Metya, A. Das and P. Talukdar, *Chem. – Eur. J.*, 2020, **26**, 8703–8708.
45 A. Kerckhoffs and M. J. Langton, *Chem. Sci.*, 2020, **11**, 6325–6331.
46 Y. R. Choi, G. C. Kim, H.-G. Jeon, J. Park, W. Namkung and K.-S. Jeong, *Chem. Commun.*, 2014, **50**, 15305–15308.
47 M. Ahmad, S. Chattopadhayay, D. Mondal, T. Vijayakanth and P. Talukdar, *Org. Lett.*, 2021, **23**, 7319–7324.
48 W.-Z. Wang, L.-B. Huang, S.-P. Zheng, E. Moulin, O. Gavat, M. Barboiu and N. Giuseppone, *J. Am. Chem. Soc.*, 2021, **143**, 15653–15660.
49 Y. Zhou, Y. Chen, P.-P. Zhu, W. Si, J.-L. Hou and Y. Liu, *Chem. Commun.*, 2017, **53**, 3681–3684.
50 C. Li, H. Chen, X. Yang, K. Wang and J. Liu, *Chem. Commun.*, 2021, **57**, 8214–8217.

51 C. Wang, S. Wang, H. Yang, Y. Xiang, X. Wang, C. Bao, L. Zhu, H. Tian and D.-H. Qu, *Angew. Chem., Int. Ed.*, 2021, **60**, 14836–14840.
52 T. Liu, C. Bao, H. Wang, Y. Lin, H. Jia and L. Zhu, *Chem. Commun.*, 2013, **49**, 10311–10313.
53 R.-Y. Yang, C. Bao, Q.-N. Lin and L.-Y. Zhu, *Chin. Chem. Lett.*, 2015, **26**, 851–856.
54 M. Ahmad, D. Mondal, N. J. Roy, T. Vijayakanth and P. Talukdar, *ChemPhotoChem*, 2022, **6**, e202200002.
55 C. Bao, M. Ma, F. Meng, Q. Lin and L. Zhu, *New J. Chem.*, 2015, **39**, 6297–6302.
56 J. Zhao, S. Lin, Y. Huang, J. Zhao and P. R. Chen, *J. Am. Chem. Soc.*, 2013, **135**, 7410–7413.
57 N. Kretschy, A.-K. Holik, V. Somoza, K.-P. Stengele and M. M. Somoza, *Angew. Chem., Int. Ed.*, 2015, **54**, 8555–8559.
58 L. Sjulson and G. Miesenböck, *Chem. Rev.*, 2008, **108**, 1588–1602.
59 S. K. Choi, M. Verma, J. Silpe, R. E. Moody, K. Tang, J. J. Hanson and J. R. Baker, *Bioorg. Med. Chem.*, 2012, **20**, 1281–1290.
60 N.-C. Fan, F.-Y. Cheng, J.-A. A. Ho and C.-S. Yeh, *Angew. Chem., Int. Ed.*, 2012, **51**, 8806–8810.
61 J. Liu, W. Bu, L. Pan and J. Shi, *Angew. Chem., Int. Ed.*, 2013, **52**, 4375–4379.
62 W. S. Shin, J. Han, R. Kumar, G. G. Lee, J. L. Sessler, J.-H. Kim and J. S. Kim, *Sci. Rep.*, 2016, **6**, 29018.
63 Y. Yang, J. Mu and B. Xing, *Wiley Interdiscip. Rev.: Nanomed. Nanobiotechnol.*, 2017, **9**, e1408.
64 W. Hou, R. Liu, S. Bi, Q. He, H. Wang and J. Gu, *Molecules*, 2020, **25**, 5147.
65 G. Jalani, V. Tam, F. Vetrone and M. Cerruti, *J. Am. Chem. Soc.*, 2018, **140**, 10923–10931.
66 R. Reinhard and B. F. Schmidt, *J. Org. Chem.*, 1998, **63**, 2434–2441.
67 S. B. Salunke, J. A. Malla and P. Talukdar, *Angew. Chem., Int. Ed.*, 2019, **58**, 5354–5358.
68 J. A. Peterson, C. Wijesooriya, E. J. Gehrmann, K. M. Mahoney, P. P. Goswami, T. R. Albright, A. Syed, A. S. Dutton, E. A. Smith and A. H. Winter, *J. Am. Chem. Soc.*, 2018, **140**, 7343–7346.
69 C. A. Lipinski, F. Lombardo, B. W. Dominy and P. J. Feeney, *Adv. Drug Delivery Rev.*, 1997, **23**, 3–25.
70 I. Aujard, C. Benbrahim, M. Gouget, O. Ruel, J.-B. Baudin, P. Neveu and L. Jullien, *Chem. – Eur. J.*, 2006, **12**, 6865–6879.
71 M. J. Hansen, W. A. Velema, M. M. Lerch, W. Szymanski and B. L. Feringa, *Chem. Soc. Rev.*, 2015, **44**, 3358–3377.
72 M. N. Chaur, D. Collado and J. M. Lehn, *Chem. – Eur. J.*, 2011, **17**, 248–258.
73 **https://app.supramolecular.org/bindfit/**.
74 A. Roy, T. Saha, M. L. Gening, D. V. Titov, A. G. Gerbst, Y. E. Tsvetkov, N. E. Nifantiev and P. Talukdar, *Chem. – Eur. J.*, 2015, **21**, 17445–17452.
75 B. L. Schottel, H. T. Chifotides and K. R. Dunbar, *Chem. Soc. Rev.*, 2008, **37**, 68–83.
76 L. E. Bickerton, A. Docker, A. J. Sterling, H. Kuhn, F. Duarte, P. D. Beer and M. J. Langton, *Chem. – Eur. J.*, 2021, **27**, 11738–11745.
77 X. Wu, E. N. W. Howe and P. A. Gale, *Acc. Chem. Res.*, 2018, **51**, 1870–1879.
78 J. T. Davis, P. A. Gale and R. Quesada, *Chem. Soc. Rev.*, 2020, **49**, 6056–6086.
79 L. Chen, S. N. Berry, X. Wu, E. N. W. Howe and P. A. Gale, *Chem.*, 2020, **6**, 61–141.
80 N. Busschaert, I. L. Kirby, S. Young, S. J. Coles, P. N. Horton, M. E. Light and P. A. Gale, *Angew. Chem., Int. Ed.*, 2012, **51**, 4426–4430.
81 P. A. Gale, C. C. Tong, C. J. E. Haynes, O. Adeosun, D. E. Gross, E. Karnas, E. M. Sedenberg, R. Quesada and J. L. Sessler, *J. Am. Chem. Soc.*, 2010, **132**, 3240–3241.
82 D. Milano, B. Benedetti, M. Boccalon, A. Brugnara, E. Iengo and P. Tecilla, *Chem. Commun.*, 2014, **50**, 9157–9160.
83 S. B. Salunke, J. A. Malla and P. Talukdar, *Angew. Chem., Int. Ed.*, 2019, **58**, 5354–5358.
84 S. O. H. Goto, N. Nakayama and K. Ohta, *CONFLEX 8*, CONFLEX Corporation, Tokyo, Japan, 2012.
85 H. Goto and E. Osawa, *J. Am. Chem. Soc.*, 1989, **111**, 8950–8951.
86 M. J. Frisch, H. B. Schlegel, G. E. Scuseria, M. A. Robb, J. R. Cheeseman, G. Scalmani, V. Barone, B. Mennucci, G. A. Petersson, H. Nakatsuji, M. Caricato, X. Li, H. P. Hratchian, A. F. Izmaylov, J. Bloino, G. Zheng, J. L. Sonnenberg, M. Hada, M. Ehara, K. Toyota, R. Fukuda, J. Hasegawa, M. Ishida, T. Nakajima, Y. Honda, O. Kitao, H. Nakai, T. Vreven, J. A. Montgomery, J. E. Peralta, F. Ogliaro, M. Bearpark, J. J. Heyd, E. Brothers, K. N. Kudin, V. N. Staroverov, T. Keith, R. Kobayashi, J. Normand, K. Raghavachari, A. Rendell, J. C. Burant, S. S. Iyengar, J. Tomasi, M. Cossi, N. Rega, J. M. Millam, M. Klene, J. E. Knox, J. B. Cross, V. Bakken, C. Adamo, J. Jaramillo, R. Gomperts, R. E. Stratmann, O. Yazyev, A. J. Austin, R. Cammi, C. Pomelli, J. W. Ochterski, R. L. Martin, K. Morokuma, V. G. Zakrzewski, G. A. Voth, P. Salvador, J. J. Dannenberg, S. Dapprich, A. D. Daniels, O. Farkas, J. B. Foresman, J. V. Ortiz, J. Cioslowski and D. J. Fox, *Gaussian 09, Revision B.01*, Gaussian, Inc., Wallingford, CT, 2010.
87 A. D. McLean and G. Chandler, *J. Chem. Phys.*, 1980, **72**, 5639–5648.
88 H. J. Cho, H. Y. Gee, K.-H. Baek, S.-K. Ko, J.-M. Park, H. Lee, N.-D. Kim, M. G. Lee and I. Shin, *J. Am. Chem. Soc.*, 2011, **133**, 20267–20276.
89 A. S. Verkman, M. C. Sellers, A. C. Chao, T. Leung and R. Ketcham, *Anal. Biochem.*, 1989, **178**, 355–361.
90 M. R. West and C. R. Molloy, *Anal. Biochem.*, 1996, **241**, 51–58.
91 A. H. Boulares, A. G. Yakovlev, V. Ivanova, B. A. Stoica, G. Wang, S. Iyer and M. Smulson, *J. Biol. Chem.*, 1999, **274**, 22932–22940.
92 V. Schreiber, F. Dantzer, J.-C. Ame and G. de Murcia, *Nat. Rev. Mol. Cell Biol.*, 2006, **7**, 517–528.
93 N. J. Curtin, *Nat. Rev. Cancer*, 2012, **12**, 801–817.
94 G. V. Chaitanya, J. S. Alexander and P. P. Babu, *Cell Commun. Signal.*, 2010, **8**, 31.

